Uptake of CO_2, SO_2, HNO_3 and HCl on Calcite ($CaCO_3$) at 300 K: Mechanism and the Role of Adsorbed Water†

Ch. Santschi and M. J. Rossi*

Laboratoire de Pollution Atmosphérique et Sol (LPAS), LPAS/ISTE/ENAC, Bâtiment de Chimie, Station 6, Ecole Polytechnique Fédérale de Lausanne (EPFL), CH-1015 Lausanne, Switzerland

Received: November 1, 2005; In Final Form: February 1, 2006

All experimental observations of the uptake of the four title compounds on calcite are consistent with the presence of a reactive bifunctional surface intermediate $Ca(OH)(HCO_3)$ that has been proposed in the literature. The uptake of CO_2 and SO_2 occurs on specific adsorption sites of crystalline $CaCO_3$(s) rather than by dissolution in adsorbed water, H_2O(ads). SO_2 primarily interacts with the bicarbonate moiety whereas CO_2, HNO_3 and HCl all react first with the hydroxyl group of the surface intermediate. Subsequently, the latter two react with the bicarbonate group to presumably form $Ca(NO_3)_2$ and $CaCl_2 \cdot 2H_2O$. The effective equilibrium constant of the interaction of CO_2 with calcite in the presence of H_2O(ads) is $\kappa = \Delta CO_2/(H_2O(ads)[CO_2]) = 1.62 \times 10^3$ bar^{-1}, where ΔCO_2 is the quantity of CO_2 adsorbed on $CaCO_3$. The reaction mechanism involves a weakly bound precursor species that is reversibly adsorbed and undergoes rate-controlling concurrent reactions with both functionalities of the surface intermediate. The initial uptake coefficients γ_0 on calcite powder depend on the abundance of H_2O(ads) under the present experimental conditions and are on the order of 10^{-4} for CO_2 and 0.1 for SO_2, HNO_3 and HCl, with γ_{ss} being significantly smaller than γ_0 for HNO_3 and HCl, thus indicating partial saturation of the uptake. At 33% relative humidity and 300 K there are 3.5 layers of H_2O adsorbed on calcite that reduce to a fraction of a monolayer of weakly and strongly bound water upon pumping and/or heating.

Introduction

Calcium carbonate occurs in three crystalline polymorphs, calcite, aragonite and vaterite, with calcite being the most stable. It is an important ubiquitous mineral in geochemical and biological systems and has found many uses in technological applications as well. In the Earth's atmosphere carbonates are a reactive component of mineral dust aerosols. For example, calcite is an important component of Saharan dust, comprising up to 30% of the aerosol mass depending on the source area.[1,2] Carbonate minerals are important in atmospheric CO_2 exchange as well as energy storage and conversion compounds. In addition, $CaCO_3$ is a major structural component of historic and contemporary building materials such as limestone, marble and sandstone, giving rise, for example, to the Egyptian pyramids, the Parthenon temple in Athens and most gothic cathedrals, respectively.

The weathering of $CaCO_3$-containing building materials or atmospheric mineral dust aerosol that is important in global climate change is intimately related to the interfacial or surface properties of the mineral itself. There is clear evidence that under ambient atmospheric conditions in the presence of CO_2 and H_2O the surface of $CaCO_3$ is terminated by OH groups that persist even under ultrahigh-vacuum conditions.[3−5] Stipp[3,4] has summarized the present knowledge about the $CaCO_3$ interface resulting from surface-sensitive spectroscopies such as atomic force microscopy (AFM), X-ray photoelectron spectroscopy (XPS), low-energy electron diffraction (LEED) and time-of-flight secondary ion mass spectrometry (TOF−SIMS), noting the abundance of chemisorbed OH^- (hydroxyl) groups opposite the Ca^{2+} ions and balanced by slightly rearranged HCO_3^- (bicarbonate) groups upon exposure of cleaved $CaCO_3$ substrates to the ambient atmosphere or bulk liquid water. There is strong evidence from XPS studies for the presence of OH and H chemisorbed at the termination of the bulk calcite structure with which all other spectroscopic results agree. Therefore, this termination layer is most conveniently described in terms of $Ca(OH)(HCO_3)$, which implies the presence of chemisorbed water. Experimental evidence from Fourier transform infrared (FTIR) absorption spectra and polarization atomic force microscopy (AFM) point toward the existence of molecularly adsorbed H_2O that support ion mobility and fast dissolution processes in carbonate materials with increasing relative humidity.[6,7] It appears that at a relative humidity of 55% an ordered molecular monolayer of H_2O is present on $CaCO_3$ and that beyond 55% relative humidity (rh) multilayer adsorption toward 3D structures is occurring. This mobile layer of adsorbed H_2O (H_2O(ads)) sits atop the chemisorbed water and partakes in interfacial chemistry akin to aqueous phase chemistry that is different from the reactions of strongly bound chemisorbed water.[7] Most importantly, the bifunctional surface adsorbate $Ca(OH)(HCO_3)$ enables the formation of the mobile layer of H_2O(ads) that is responsible for much of the chemistry at high relative humidity at atmospheric conditions.

In contrast, the present work explores the reactivity of the reactive bifunctional surface intermediate as a function of the abundance of adsorbed water. It addresses the mechanism of the interfacial chemistry of $CaCO_3$ in the presence of important atmospheric trace gases that corrode or chemically react with $CaCO_3$ such as CO_2, SO_2 and atmospheric acidity such as HNO_3 and HCl. $CaCO_3$ has a modest solubility in H_2O amounting to 1.4×10^{-3} g L^{-1}. However, in the presence of H_2O and CO_2

† Part of the special issue "David M. Golden Festschrift".

* To whom correspondence should be addressed. E-mail: michel.rossi@epfl.ch.

10.1021/jp056312b CCC: $33.50
Published on Web 02/28/2006

the following equilibrium is established on solid $CaCO_3$, which leads to its dissolution:

$$CaCO_3(s) + CO_2(g) + H_2O(ads) \leftrightarrows Ca^{2+}(aq) + 2HCO_3^-(aq) \quad (1)$$

This equilibrium shows that CO_2 in conjunction with H_2O can be corrosive with respect to solid $CaCO_3$(s) and is involved in Karst dissolution. It plays an important role in global carbon cycles involving atmospheric water and CO_2.[8] Despite the modest solubility of $CaCO_3$ in pure water, most carbonate minerals readily dissolve in acidic aqueous solution by forming soluble calcium bicarbonate upon the combined action of acidity, H_2O and CO_2 according to the following equilibrium reactions:[9,10]

$$CaCO_3(s) + H^+(aq) \leftrightarrows Ca^{2+}(aq) + HCO_3^-(aq) \quad (2)$$

$$CaCO_3(s) + H_2CO_3 \leftrightarrows Ca^{2+}(aq) + 2HCO_3^-(aq) \quad (3)$$

CO_2 is an important greenhouse gas that also plays a vital role in the biosphere in terms of assimilation and transpiration reactions. In aqueous solutions CO_2 plays an important role in the dissolution of carbonate minerals,[10,11] which again feed back into global carbon cycles in the atmosphere.[8]

The sources of sulfur in the atmosphere primarily stem from biogenic and fossil fuel burning of S-containing hydrocarbons in addition to occasional volcanic eruptions. SO_2 is the main oxidation product and is a precursor to H_2SO_4, which together with HNO_3 is one of the most important acidic compounds in the atmosphere. The oxidation of SO_2 in the atmosphere takes place both homogeneously by reaction with OH and heterogeneously on aerosol surfaces. For instance, oxidation of SO_2 in the marine troposphere takes place up to 60% on aerosols.[12] The water content of calcite particles is important in the atmospheric oxidation of SO_2 that may proceed via the formation of a crystalline calcium sulfite hemihydrate,[12] hence our emphasis on the role of adsorbed water in the present study.

Atmospheric pollution most often is accompanied by the presence of atmospheric acidity that is partially neutralized by NH_3, which leads to aerosol formation. Surface chemistry of $CaCO_3$ with acidic trace atmospheric gases such as HNO_3 and SO_2 has been investigated using FTIR absorption and surprisingly revealed adsorbed H_2CO_3 that is stable on the surface of calcite and that may be involved in surface chemistry of $CaCO_3$.[7] The presence of HNO_3 in today's urban polluted atmosphere has taken precedence over H_2SO_4 and is principally due to the increase of the abundance of NO_x in comparison to the recent decrease of SO_2 levels. HCl occurs in the remote marine boundary layer where it plays a role in halogen activation reactions of sea salt as well as in urban polluted areas where it can reach up to 3 ppb.[13] Important HCl sources are coal combustion, municipal waste incineration (PVC) and occasional volcanic eruptions.

Triggered by the importance of mineral dust with respect to atmospheric composition change and cloud condensation/formation on mineral dust particles[14] several kinetic studies of trace gases with calcite and authentic mineral dust have been performed in the recent past. The interaction of SO_2 with both $CaCO_3$ and Saharan dust has been studied over a range of pressures.[7,15−18] The uptake of HNO_3 on $CaCO_3$ and Saharan dust has garnered sustained interest over the years because of the strong interaction of this trace gas with mineral dust.[7,19−24] In addition, two recent studies on the interaction of H_2O with Saharan dust have been performed.[25,26] The present work reports on the uptake kinetics and mechanism of four important atmospheric trace gases, namely, CO_2, SO_2, HNO_3 and HCl that are all corrosive or reactive with respect to calcite. The emphasis was placed on the common chemical mechanism and on the importance of adsorbed water.

TABLE 1: Parameters of the Used Knudsen Reactor

parameter	value
reactor volume	1830 cm^3
estimated internal surface area	1300 cm^2
sample compartment surface area	19.6 cm^2
chopper frequency	70 Hz
orifice o.d. (nominal)	1, 4, 8 and 14 mm
collision frequency $\omega = (8RT/\pi M)^{1/2}(A_S/4V)$	$39(TM^{-1})^{1/2}$ [a]
escape rate constant k_{esc}[b]:	
1 mm orifice	$0.01(TM^{-1})^{1/2}$ s^{-1}
4 mm orifice	$0.24(TM^{-1})^{1/2}$ s^{-1}
8 mm orifice	$0.79(TM^{-1})^{1/2}$ s^{-1}
14 mm orifice	$1.77(TM^{-1})^{1/2}$ s^{-1}

[a] ω calculated for the geometrical surface area of the sample (19.6 cm^2). [b] Experimentally determined values. T (K) and M (g mol^{-1}) are temperature and molecular mass, respectively.

Experimental Details

All experiments have been performed using a Knudsen flow reactor equipped with mass spectrometric (MS) detection that has been pioneered by Golden, Spokes and Benson.[27] A two-chamber version adapted to the study of heterogeneous reactions has been described in detail in the recent literature.[28] Measured flows of gases are admitted across a flow-controlling needle valve or a glass capillary connecting the stagnant volume to the two-chamber Knudsen reactor that subsequently reacted with the active substrate once the isolation plunger was lifted. The use of several escape apertures leading to different gas residence times $\tau_g = 1/k_{esc}$, where k_{esc} is the measured effusion rate constant, constitute independent data sets that are used to unravel the rate law of the heterogeneous reaction. The kinetics are expressed as a heterogeneous rate constant k_{het} that depends on the surface-to-volume ratio A_s/V of the specific measurement system or as a dimensionless uptake coefficient γ that has been normalized by A_s/V on the basis of the geometric surface area and is therefore a transferable parameter.

$$k_{het} = (I_0/I - 1)k_{esc} \quad (4)$$

$$\gamma = k_{het}/\omega \quad (5)$$

where I_0 and I are the rectified amplitudes of the MS signals of the chopped molecular beam recorded by the lock-in amplifier in the absence and presence of the sample, respectively, and $\omega = (\langle c \rangle/4V)A_s$ is the calculated gas−surface collision frequency of the average molecule moving at a molecular speed $\langle c \rangle$. The uptake coefficient γ therefore determines the net loss of a molecule M from the gas phase over a gas lifetime spanning a factor of 250, typically from 0.1 to 25.0 s for the average molecule M. The specific parameters of the used Knudsen flow reactor are given in Table 1.

Both CO_2 (Carbagas SA) and SO_2 (Matheson Inc.) were used without further purification by filling a storage volume at typically several Torr. MS analysis has not indicated impurity levels above 100 ppm. HCl was been synthesized from the reaction of concentrated sulfuric acid (95%, 5% H_2O, Fluka AG) with dry NaCl (Fluka AG, puriss.) at ambient temperature under vacuum conditions (10^{-2} Torr) according to

$$H_2SO_4(l) + 2NaCl(s) \rightarrow 2HCl(g) + Na_2SO_4(s) \quad (6)$$

The gaseous HCl has been trapped at 77 K and subsequently transferred into a Pyrex bulb for storage at several Torr. The purity of HCl was checked using MS as indicated above.

HNO_3 has been prepared by mixing concentrated HNO_3 (Fluka AG, 99.5%) with concentrated H_2SO_4 (95%, Fluka AG) in a volume ratio 1:3 v/v and taking the equilibrium vapor pressure of HNO_3 above the liquid. Before carrying out an experiment, the liquid H_2SO_4/HNO_3 mixture has been purged by bubbling N_2 for 10 min to rid the solution of NO_2. The main peaks in the MS spectrum of HNO_3 are at *m*/*e* 63 (molecular ion, 1.0%), *m*/*e* 46 (base peak, 100.0%) and *m*/*e* 30 (fragment, 60.0%).

The uptake experiments have been carried out on two types of precipitated $CaCO_3$, which corresponds to the thermodynamically stable mineral calcite; one we call high ordered (99.5% purity, Merck AG), the other low ordered (puriss., Fluka AG) in reference to the structure. The high-ordered sample consists of more or less regular cubic or rhomboedric crystals with $d = 2\ \mu$m sides, as revealed by SEM whereas the low-ordered $CaCO_3$ is irregular in shape. Unless indicated otherwise all uptake experiments have been performed on high-ordered $CaCO_3$. The BET surface determined using a Sorptomatic 1990 instrument (Fisons Inc.) resulted in values of 3.7 and 5.1 $m^2\ g^{-1}$ for the high- and low-ordered sample, respectively, when a cross-sectional area of 16.2 $Å^2$ for N_2 is used.[29] The conditioning of the samples prior to the BET measurement involved heating of the samples for 3.5 and 2.5 h at 50 and 250 °C, respectively. The apparent density of the $CaCO_3$ powder has been determined by measuring the weight of a known volume and resulted in $\rho_p = 1.3\ g\ cm^{-3}$ in comparison with the true density of $\rho = 2.9\ g\ cm^{-3}$ given by the supplier. Using a cubic box approximation for the individual particles of high-ordered $CaCO_3$ of the form $A_s = A_v/\rho_p = 6/\rho d$, we obtain the dimension $d = 0.56\ \mu$m of the cubic particles, where A_s and A_v are the total surface area per gram (corresponding to the BET surface area) and per cm^3, respectively. This also corresponds to the surface-to-mass ratio of an individual particle. The discrepancy between this value and the one from the inspection of the SEM image indicates some roughness of the cubic crystal faces in addition to the slightly polydisperse nature of the crystalline sample.

Owing to the importance of H_2O for the mechanism of heterogeneous interaction with trace gases we have evaluated the water content of high-ordered precipitated $CaCO_3$ at 33% relative humidity and 294 K by introducing a weighed amount, typically 12−14 g of $CaCO_3$(s), into a closed metallic tube of 7.5 cm^3 volume that was subsequently weighed using a Mettler Toledo AE 240 balance. The partially filled tube was then connected to the 14 mm orifice flow reactor and heated until the *m*/*e* 18 water signal reached background level, after which the closed tube was weighed again. Repeated difference measurements before and after baking resulted in $m_{H_2O} = 4.0 \pm 0.5$ mg of H_2O/g of $CaCO_3$(s) with the buoyancy correction amounting to less than 10%. Therefore, the measured mass of adsorbed H_2O of 4 ± 0.5 mg/g corresponds to 3.5 formal monolayers of adsorbed water at ambient temperature and pressure at 33% rh using a BET surface area of 3.7 $m^2\ g^{-1}$ and 1×10^{15} molecule cm^{-2} as a formal monolayer of H_2O on calcite in analogy to ice.

Crystalline $CaCO_3$ samples (Italian Carrara marble) were cut into 5 mm thick 50 mm diameter disks that were heated in an oven at 330 K for 24 h prior to use as the bulk Carrara marble has been stored in water. Occasionally, the cut (rough) marble samples have been polished down to a roughness of 6 μm using several grades of polishing paper. The total exposed geometric surface was 27.4 cm^2 consisting of the top and the side surface.

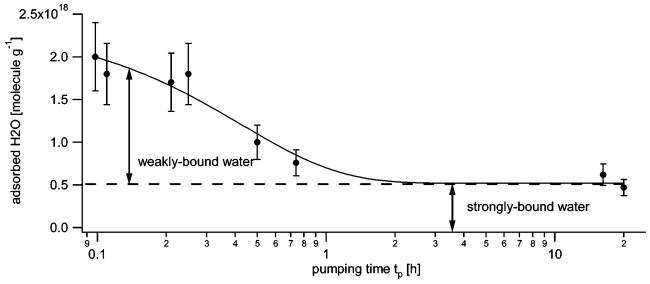

Figure 1. Amount of adsorbed water on precipitated $CaCO_3$ as a function of pumping time at ambient temperature using the 14 mm diameter orifice reactor. The curve interpolates the data points and serves to guide the eye.

For water desorption experiments from precipitated $CaCO_3$ a gold-coated all-metal sample holder was used for the kinetic experiments. Prior to a sample run a blank was performed with the empty sample holder that obtained 2×10^{16} molecules of adsorbed H_2O after 30 min of pumping at ambient temperature followed by heating to 600 K. This corresponds to less than 1% of the quantity of adsorbed H_2O on $CaCO_3$.

Results and Discussion

H_2O Adsorbed on Precipitated $CaCO_3$(s) Powder. Surface adsorbed H_2O plays a crucial role in the heterogeneous reactions of acidic trace gases on $CaCO_3$ substrates. To gauge the importance of adsorbed H_2O under the present low-pressure experimental conditions, we have carried out in situ H_2O desorption experiments from calcite powder at various stages of pumping to quantitatively measure the amount of adsorbed water H_2O(ads) as a function of pumping time. The present Knudsen flow reactor is characterized by rather low volumetric pumping rates that are given by Vk_{esc}, which range from 0.2 to 40 L s^{-1} for the 1 and 14 mm diameter orifices, respectively. In the following, the samples have always been pumped initially at approximately 40 L s^{-1} prior to an uptake experiment of CO_2 that ordinarily took place at a much smaller pumping rate (=orifice diameter). To minimize additional desorption of H_2O originating from the sample support, we have used an all-metal (Au coated) sample holder described in ref 28.

The experimental protocol consisted of pumping 1 g of precipitated $CaCO_3$ for a given time t_p at ambient temperature using the 14 mm diameter orifice reactor. Subsequently, the sample was heated to $T = 470$ K for as long as it took to return the MS signal at *m*/*e* 18 to background level. During the whole experiment the MS signal at *m*/*e* 18 was recorded and the integration was performed from t_p to the end of the experiment. Figure 1 displays the remaining H_2O adsorbed on $CaCO_3$ as a function of pumping time t_p in the 14 mm orifice reactor. We call the residual H_2O level of 5×10^{17} molecule g^{-1} that remains after 20 h of pumping at ambient temperature "strongly bound H_2O" because it desorbs only at high temperature whereas the quantity of H_2O(ads) exceeding this level is called henceforth "weakly bound water", as displayed in Figure 1. Precipitated $CaCO_3$(s) contains 4 mg g^{-1} of adsorbed H_2O at ambient atmospheric conditions (33% rh, 294 K) corresponding to 1.34×10^{20} molecules g^{-1}, which decreases to 2×10^{18} molecules g^{-1} after 6 min of pumping. This pumping time at ambient temperature is sufficient to remove 98.5% of adsorbed water from the hydrated surface. Figure 1 reveals 5×10^{17} of adsorbed H_2O molecules g^{-1} corresponding to 1.35×10^{13} H_2O cm^{-2}

after 2 h of pumping that persist even after 20 h of pumping. These strongly bound H_2O molecules represent 0.4% of the total H_2O adsorbed at ambient conditions. Previously, experimental and theoretical studies have indicated an ordered two-dimensional icelike structure for the first H_2O layer adsorbed on calcite,[3,30,31] which will lead to a surface density of 1×10^{15} molecule cm^{-2} for H_2O if we take typical data for water ice. This leads to 3.5 monolayers of adsorbed water on high-ordered calcite at ambient conditions (33% rh, 300 K), to 5.4% of a monolayer after 6 min of pumping and to 1.4% of a monolayer of strongly bound or chemisorbed H_2O.

De Leuuw and Parker[5,30] concluded from their theoretical model that the molecularly adsorbed water on low-index surfaces of calcite and aragonite was hydrogen bonded. The same conclusion was reached in an AFM study of calcite interacting with H_2O vapor.[32] *In situ* X-ray reflectivity measurements indicated that exposure of calcite to water vapor at ambient temperature resulted in a thin film of water of 19.9 Å thickness that corresponds to 5 molecular monolayers,[33] a result that is consistent with 3.5 monolayers at rh = 33% obtained in this work. Polarization atomic force microscopy on calcite that measures the mobility of surface ions in an electric field imposed by the probe tip revealed a distinct change of the structure of the mobile molecularly adsorbed H_2O layer when the relative humidity was increased beyond 55%.[6] Below this value an ordered icelike 2D island structure seems to prevail until a monolayer at rh = 55% is obtained. Beyond this value multilayer adsorption of H_2O occurs with a 3D-structure resembling liquid water. This result is consistent with FTIR absorption of calcite powder as a function of rh where shifts and bandwidths of the OH-stretching region of H_2O(ads) have been monitored.[7] The molecular picture of a calcite surface in the presence of water vapor that emerges from the foregoing is that a mobile molecularly adsorbed H_2O(ads) layer overlays a chemisorbed water layer represented by a bifunctional surface intermediate $Ca(OH)(HCO_3)$ that caps the solid substrate.

The bifunctional surface intermediate $Ca(OH)(HCO_3)$ that seems to be responsible for the interfacial reactivity of calcite in the absence of a large part of H_2O(ads) is part of the hydrated layer supported by $CaCO_3$(s). However, it is not possible to unambiguously identify the surface intermediate as the strongly bound H_2O shown in Figure 1 on the basis of the present experiments. By following the curve in Figure 1 to longer pumping times, one sees that strongly bound H_2O persists whereas yields and kinetics of uptake reactions to be discussed depend on the amount of H_2O(ads). However, it is possible that, by pumping off weakly bound H_2O displayed in Figure 1, one converts part of the bifunctional surface intermediate in a slow reaction toward nonreactive $CaCO_3$(s) according to

$$Ca(OH)(HCO_3) \rightarrow CaCO_3(s) + H_2O \qquad (7)$$

The present results are at variance with the results obtained by thermogravimetric analysis (TGA) obtained by Gustafsson et al.[26] who obtain 0.7 monolayers of adsorbed water on calcite at 33% rh and ambient temperature. However, the present results may not be comparable to those of Gustafsson et al.[26] because these authors conditioned their samples prior to TGA analysis at 120 °C in He "to remove any species adsorbed on the surface".

Adsorption of CO_2. Uptake experiments of CO_2 on 30 g of precipitated $CaCO_3$ have been performed in the 1 mm orifice reactor during typically 1500 s as displayed in Figure S1 (Supporting Information). The uptake of CO_2 saturates at long exposure times. After closing the sample compartment, halting the CO_2 inflow and reopening the sample compartment after approximately 200 s desorption of some CO_2 has been observed using the 14 mm orifice reactor resulting in a constant yield ratio of molecules (lost/recovered) = 4/1. The fact that only 25% of the integral amount of the initially adsorbed CO_2 is recovered suggests fast initial formation of a weakly bound surface intermediate species and a slower secondary reaction of the CO_2-containing intermediate. The influence of H_2O adsorbed on $CaCO_3$, H_2O(ads), has been investigated by performing uptake experiments of CO_2 on $CaCO_3$ that has been pumped prior to uptake for a variable length of time. The amount of H_2O(ads) as a function of pumping time is given in Figure 1. Figure 2a displays the amount of CO_2 taken up and recovered by desorption as a function of H_2O(ads) at $[CO_2] = 7 \times 10^{12}$ molecule cm^{-3}. The net amount of "strongly" bound CO_2 corresponds to the difference of both lines in Figure 2a and linearly increases with H_2O(ads). This result suggests that the number of CO_2 adsorption sites on $CaCO_3$ is linearly related to H_2O(ads). In ancillary experiments we have found that the amount of both adsorbed and desorbed CO_2 linearly scales with the mass of $CaCO_3$ in the range 0−30 g, which means that the total mass of the substrate partakes in the CO_2 uptake and desorption on the time scale of the experiment (1500 s).

Most of CO_2 dissolved in bulk H_2O(l) remains in the form of dissolved gas CO_2(aq) rather than as hydrated carbonic acid, H_2CO_3(aq), which is present at less than 1% in solution at ambient temperature.[34−36] The first-order rate constant for the formation of H_2CO_3(aq) has been measured as 3×10^{-3} s^{-1} at 298 K which indicates a rather sluggish reaction in the bulk aqueous phase.[37] Henry's law constant $K_H(CO_2) = [CO_2(l)]/P(CO_2) = 0.035$ mol L^{-1} bar^{-1} for the dissolution of CO_2 in H_2O with $[CO_2(l)]$ and $P(CO_2)$ in mol L^{-1} and bar, respectively, indicates a modest solubility of CO_2 in bulk water.[38] We will in the following examine whether the amount of H_2O(ads) on $CaCO_3$ is sufficient to dissolve the amount of lost CO_2 using the results of Figure 2a and $K_H(CO_2)$. At 1.5×10^{18} H_2O(ads) g^{-1}, corresponding to a pump down time of 12 min for $CaCO_3$, Figure 2a displays a net CO_2 loss $\Delta CO_2 = 7.1 \times 10^{14}$ g^{-1} at $[CO_2] = 7 \times 10^{12}$ molecule cm^{-3} when we take the recoverable quantity of CO_2 from curve (b) in Figure 2a as the amount that remains "dissolved" in contrast to the reacted fraction. At this $[CO_2]$ we calculate an aqueous phase concentration of $[CO_2(l)] = K_H(CO_2)\ P(CO_2) = 6.12 \times 10^{15}$ CO_2 molecules L^{-1} at saturation, which has to be contrasted with the net loss of 7.1×10^{14} CO_2 g^{-1} of $CaCO_3$ in the presence of 1.5×10^{18} H_2O(ads) g^{-1}. When we divide the amount of CO_2 lost per gram of $CaCO_3$ by the quantity of CO_2 that dissolves in 1 L of H_2O according to Henry's law, that is, $7.1 \times 10^{14}/6.12 \times 10^{15}$, we obtain the volume of H_2O needed to dissolve ΔCO_2, 116 mL of H_2O or 3.9×10^{24} H_2O g^{-1}. This is clearly at variance with the amount of H_2O(ads) = 1.5×10^{18} g^{-1} remaining on $CaCO_3$ after 12 min of pumping. One would need a factor of 2.6×10^6 ($=3.9 \times 10^{24}/1.5 \times 10^{18}$) more H_2O to dissolve ΔCO_2, the measured net CO_2 taken up on $CaCO_3$ if it were a regular aqueous solution of CO_2. Therefore, the $CaCO_3$ substrate must have specific adsorption sites that accommodate CO_2 beyond the regular aqueous dissolution process.

We identify the reactive intermediate with the bifunctional surface species presented in the review of Stipp et al.,[3] which results from the interaction of CO_2/H_2O with $CaCO_3$ surfaces according to eq 8 as briefly discussed above: Reaction 8

$$CaCO_3(s) + H^+(aq) + HCO_3^-(aq) \leftrightarrows Ca(OH)(HCO_3) + CO_2 \qquad (8)$$

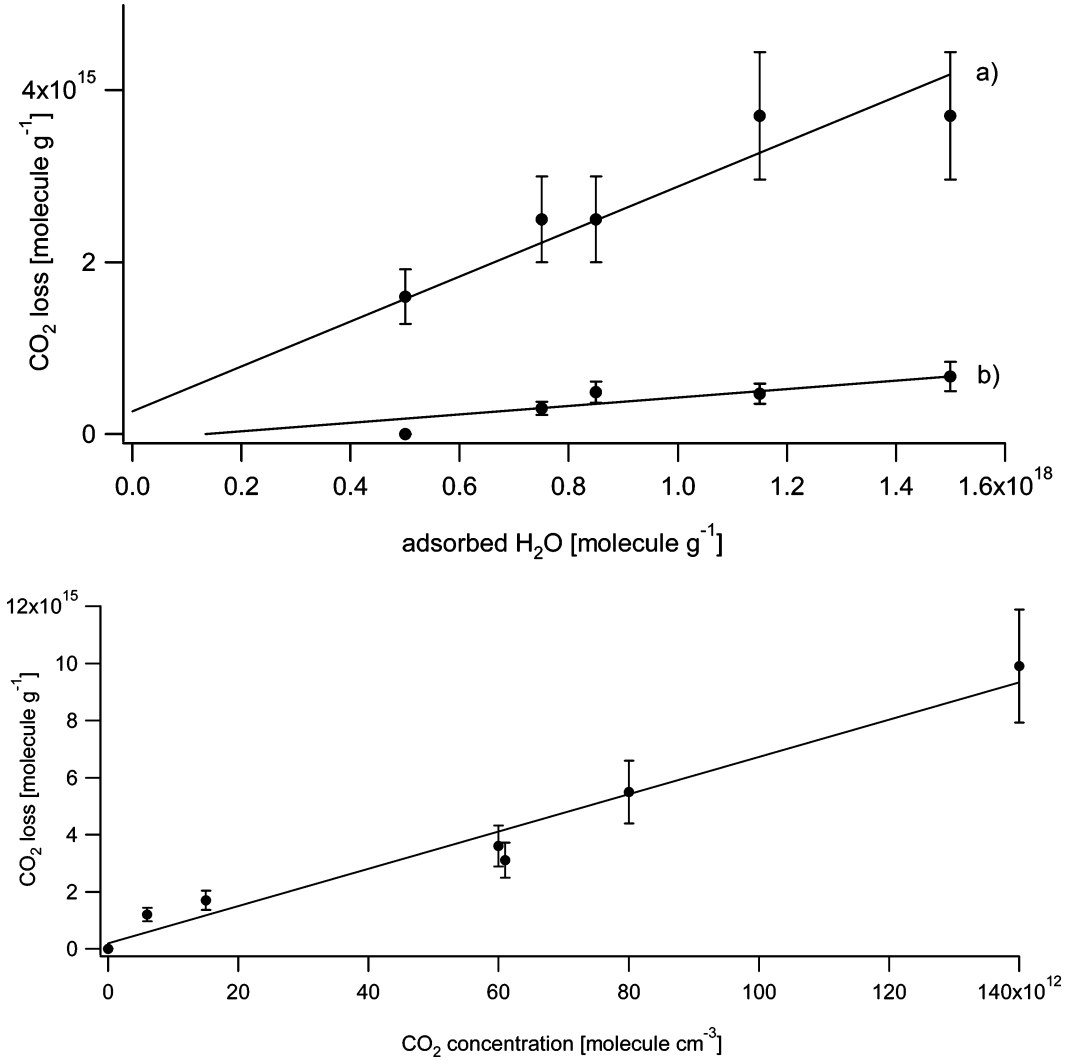

Figure 2. (a) Total amount of CO_2 taken up (a) and the recovered amount (b) of CO_2 interacting with 1 g of precipitated $CaCO_3$ in the 1 mm orifice reactor at $[CO_2] = 7 \times 10^{12}$ molecule cm^{-3}. The difference between (a) and (b) separated by a waiting period of 90 s indicates the amount of CO_2 permanently adsorbed on the sample. (b) Total amount of adsorbed CO_2 displayed as a function of $[CO_2]$ from uptake experiment performed in the 1 mm orifice reactor in the presence of 1 g of precipitated $CaCO_3$. The amount of adsorbed H_2O was 1.1×10^{18} molecule g^{-1}.

effectively amounts to chemisorption of water on calcite thereby releasing CO_2 that was used to create the bicarbonate ion through dissociation of carbonic acid, H_2CO_3. It is reasonable to assume that the mobile layer of molecularly adsorbed water behaves like bulk as far as CO_2 dissolution is concerned such that the large CO_2 uptake may totally be attributed to the presence of the bifunctional surface intermediate. The above loss of 7.1×10^{14} CO_2 g^{-1} for high-ordered $CaCO_3$ corresponds to a surface density of 1.9×10^{10} adsorption sites cm^{-2} for CO_2, which is approximately 2.5 orders of magnitude smaller than the quantity of chemisorbed, that, is strongly bound, water of 1.35×10^{13} H_2O cm^{-2} (see above). The reaction mechanism of CO_2 with the surface intermediate $Ca(OH)(HCO_3)$ is displayed in reactions 9 and 10 with reaction 10 being the slow, that is, rate-limiting,

$$Ca(OH)(HCO_3) + CO_2(g) \leftrightarrows Ca(OH)(HCO_3){-}CO_2 \quad (9)$$

$$Ca(OH)(HCO_3){-}CO_2 \rightarrow Ca(HCO_3)_2 \quad (10)$$

step. The fact that only 25% of the adsorbed CO_2 may be recovered indicates that the major part of the consumed CO_2 undergoes a chemical reaction, most probably to calcium bicarbonate whose stability may be enhanced at the gas−solid interface. Reaction 10 is the only rational pathway because the reaction of CO_2 with the bicarbonate moiety does not lead to a stable intermediate. In principle, CO_2 adsorption to $CaCO_3$ may also proceed via the reverse of reaction 8, resulting in adsorbed H_2CO_3. However, we do not expect a net uptake of CO_2 owing to the instability of H_2CO_3 in the presence of H_2O(ads), as it will quickly dissociate into CO_2 and H_2O(ads) given its significant excess with respect to $Ca(OH)(HCO_3)$. In addition, the uptake of CO_2 clearly saturates at long reaction times, as displayed in Figure S1. Once the bifunctional surface intermediate $Ca(OH)(HCO_3)$ has been consumed net CO_2 uptake ceases according to reactions 9 and 10.

Prolonged pumping may be accompanied by the irreversible destruction of the bifunctional surface intermediate $Ca(OH)(HCO_3)$ by evaporation of H_2O according to reaction 7. The irreversible nature of this reaction on the time scale of the uptake experiment stems from the fact that reaction 8 seems to be slow under the present low-pressure conditions. It apparently only takes place at ambient conditions of high partial pressure of H_2O and CO_2 but not under flow reactor conditions, as we could never measure uptake of H_2O. Once H_2O(ads) has been removed by pumping and heating, an irreversible change of the substrate surface has obviously taken place that prevents it from reacting with atmospheric trace gases.

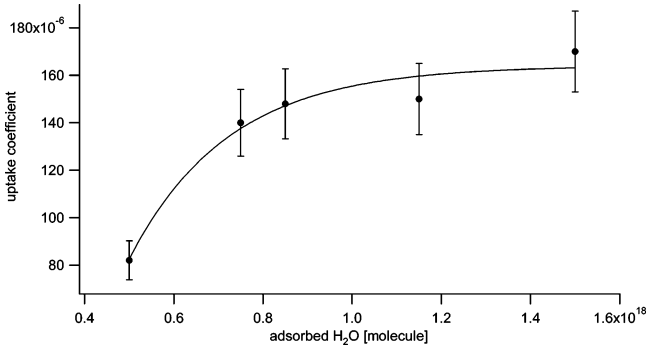

Figure 3. Initial uptake coefficient γ_0 of the reaction of CO_2 with 1 g of precipitated $CaCO_3$ as a function of the amount of adsorbed H_2O performed in the 1 mm orifice reactor at $[CO_2] = 7 \times 10^{12}$ molecule cm^{-3}.

The dependence of the amount of adsorbed CO_2 on $[CO_2]$ is displayed in Figure 2b. Every uptake experiment has been performed on a fresh $CaCO_3$(s) sample, each with the same amount of H_2O(ads). The amount of adsorbed CO_2 linearly increases with $[CO_2]$ at constant H_2O(ads). The slope of the straight line plotted in Figure 2b corresponds to the partition constant between gas and adsorbed CO_2 and assumes the value of 65.7 cm^3/g for $H_2O(ads) = 1.1 \times 10^{18}$ molecules per g of $CaCO_3$(s). The H_2O(ads) dependence may be understood as a family of linear curves of the type displayed in Figure 2b whose slopes linearly scale with H_2O(ads). We would like to emphasize that this system obviously does not correspond to a simple Henry's law for CO_2 dissolution. Rather, a "preequilibrium" of H_2O adsorption must precede the adsorption of CO_2(g) in which the Henry's law constant describing the interaction $CO_2(g) \leftrightarrows CO_2(aq)$ has to be folded with the equilibrium $H_2O(g) \leftrightarrows H_2O$(ads). When we take the data displayed in Figure 2a,b and express the amount ΔCO_2 of CO_2 adsorbed to $CaCO_3$(s) in molecule g^{-1} with respect to both the amount of adsorbed water H_2O(ads) in molecule g^{-1} and the gas-phase concentration $[CO_2]$ in bar in terms of an overall equilibrium constant κ, we obtain $\kappa = \Delta CO_2/(H_2O(ads)\ [CO_2]) = 1.62 \times 10^3\ bar^{-1}$ at 300 K. This is a transferable thermodynamic constant because the ratio of both ΔCO_2 and H_2O(ads) have been normalized to 1 g of $CaCO_3$.

Figure 3 displays the dependence of the initial uptake coefficient γ_0 on the amount of H_2O(ads) measured in the 1 mm orifice reactor. As expected, γ_0 increases monotonically over the examined range of H_2O(ads) and starts to saturate at higher values of H_2O(ads). This behavior is consistent with the deactivation of the $CaCO_3$ surface upon pumping off adsorbed H_2O according to reaction 7 thereby decreasing the number of adsorption sites on $Ca(OH)(HCO_3)$. The displayed γ values are initial uptake coefficients γ_0 that have not been corrected for pore diffusion because CO_2 is unlikely to explore the total internal surface as given by the BET area on the time scale given by $1/k_{esc}$. However, we regard these values as upper limits to the true γ values.[24,39]

The uptake of CO_2 on hydrated $CaCO_3$(s) is consistent with the presence of the reactive bifunctional intermediate $Ca(OH)(HCO_3)$ in addition to weakly bound, that is, hydrogen-bonded, H_2O making up the mobile or molecularly adsorbed H_2O. The former is generated at ambient atmospheric conditions and is presumably converted into nonreactive $CaCO_3$(s) according to reaction 7 upon evaporation of H_2O through prolonged pumping. On the basis of the comparison with the known Henry's law constant of physical dissolution of CO_2 in H_2O, it is obvious that adsorption of CO_2, which strongly depends on H_2O(ads), involves specific interaction with a surface intermediate. The interaction with CO_2(g) therefore does not occur through physical dissolution of CO_2(g) in H_2O(ads) but rather through adsorption on specific surface sites. It seems that maintaining the hydration layer at the gas−solid interface of $CaCO_3$(s) is crucial for maintaining surface reactivity in terms of the concentration of $Ca(OH)(HCO_3)$, the site of CO_2 adsorption.

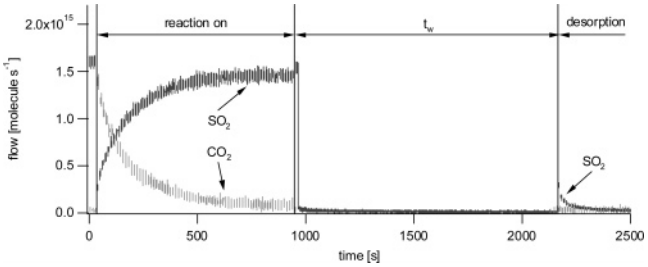

Figure 4. Uptake experiment of SO_2 ($m/e = 64$) on 1 g of precipitated high-ordered $CaCO_3$ performed in the 14 mm orifice reactor. CO_2 has been observed as reaction product. After isolation of the sample and a waiting period t_w of 20 min the sample compartment was opened and desorption of SO_2 recorded.

Adsorption of SO_2. The uptake of SO_2 on high-ordered $CaCO_3$(s) was studied in the 14 mm orifice reactor owing to its large value and CO_2 was observed as its unique gas-phase product. A typical uptake experiment is displayed in Figure 4. Prior to each uptake experiment the $CaCO_3$(s) sample has been pumped for 30 min, which leaves 1.1×10^{18} molecule g^{-1} of H_2O(ads) or 3% of a formal monolayer on the calcite according to Figure 1. Immediately after lifting the isolation plunger, CO_2 is formed at once at high rates compared to the rate of escape, $k_{esc}[CO_2]$. Complete saturation of the SO_2 uptake sets in after 15 min once approximately 2.7×10^{17} SO_2 g^{-1} or 7.3×10^{12} molecules cm^{-2} of SO_2 are taken up, and CO_2 decreases to the background level at the same time. After a waiting period of $t_w = 20$ min during which the sample compartment was isolated from the gas flow, the isolation plunger was lifted and desorption of a small amount of SO_2 was observed (Table 2, experiment 1a). The mass balance of all experiments performed on high-ordered $CaCO_3$(s) has resulted in a 1:1 correspondence of SO_2 lost vs CO_2 formed where SO_2 lost is equal to SO_2 initially adsorbed minus SO_2 recovered by desorption.

Akin to CO_2, SO_2 has only a modest solubility in water at 298 K expressed as a Henry's law constant $K_H(SO_2) =$ of 1.3 mol L^{-1} bar^{-1}.[38] Under the conditions of Figure 4 $[SO_2] = 2.3 \times 10^{11}$ molecule cm^{-3} at a flow rate into the reactor of 1.6×10^{15} molecule s^{-1}. At this $[SO_2]$ 1 L of H_2O is able to dissolve $K_H(SO_2)\ P(SO_2) = 7.5 \times 10^{15}$ SO_2 L^{-1} at saturation. The recoverable quantity $\Delta SO_2 = 8 \times 10^{16}$ SO_2 g^{-1} may be obtained from Figure 6 for $t = 0$ and corresponds to the integral under the SO_2 uptake curve displayed in Figures 4 and 5 extrapolated to $t = 0$. The dissolution of ΔSO_2 at $[SO_2] = 2.3 \times 10^{11}$ molecule cm^{-3} requires 10.7 L g^{-1} of liquid H_2O corresponding to 3.6×10^{26} H_2O g^{-1}. This massive imbalance of roughly 8 orders of magnitude between the required amount of H_2O, based on Henry's law, and available $H_2O(ads) = 1.1 \times 10^{18}$ H_2O g^{-1} reveals the presence of specific adsorption sites for SO_2 as was the case for CO_2. This imbalance is more pronounced for SO_2 than for CO_2 owing to the larger value of ΔSO_2 compared to ΔCO_2.

To probe the possible surface regeneration as far as SO_2 uptake is concerned, a poisoned sample was pumped for 8 h, after which an additional uptake experiment was performed (Table 2, experiment 1b). Additional uptake of SO_2 was observed, but no formation of CO_2. When the amount of SO_2

TABLE 2: Typical Experimental Conditions and Main Results of SO_2 Uptake Experiments on Precipitated High-Ordered $CaCO_3$(s)

no.	orifice diameter (mm)	[SO_2] (molecule cm^3)	experimental conditions	uptake kinetics	remarks
1a	14	2.2×10^{11}	estimated amount of H_2O: 1.1×10^{18} molecule	$\gamma_0 = 0.13$	mass balance: 1 mol of $SO_2 \rightarrow$ 1 mol of CO_2 desorption of SO_2 yield of CO_2: 2.7×10^{17} molecule
1b	14	2.2×10^{11}	saturated sample pumped overnight	$\gamma_0 = 0.12$	no CO_2 mss balance: loss of 65% of the total amount of adsorbed SO_2, which is 1.1×10^{17}molecule
1c	14	2.2×10^{11}	stocked at ambient conditions for 5 days after saturation same conditions as for 1a	$\gamma_0 = 0.13$	mass balance: 1 mol of $SO_2 \rightarrow$ mol of CO_2 desorption of SO_2 yield of CO_2: 7×10^{16} molecule
2	14	2.2×10^{11}	estimated amount of H_2O: 1.1×10^{18} molecule		amount of recoverable SO_2 decreases exponentially with t_w
3	14	2.2×10^{11}	experiment on $Ca(OH)_2$	$\gamma = 0.4$	no products and no desorption of SO_2 observed no saturation within 15 min
4	14	1.5×10^{11}	not saturated, low-ordered sample	$\gamma_0 = 0.2$	1.5 mol of $SO_2 \rightarrow$ 1 mol of CO_2 yield of CO_2: 2.7×10^{17} molecule
5	14	2.2×10^{11}	estimated amount of H_2O: 1.1×10^{18} and 5×10^{17} molecules	$\gamma_0 = 0.2$ $\gamma_0 = 0.1$	initial uptake coefficient is higher for the sample containing more H_2O(a) formation of CO_2 3×10^{17} and 2.5×10^{17} molecules for high and low water levels, respectively

desorbing after $t_w = 5$ min was compared to the quantity of SO_2 adsorbed, we concluded that net SO_2 adsorption had taken place where 45% of the total adsorbed SO_2 had been recovered from a saturated sample of $CaCO_3$(s). The result is that surface sites leading to loss of SO_2 may regenerate whereas reactive sites leading to formation of CO_2 remain saturated under flow reactor conditions. This result is at variance with Adams et al. who did not observe recovery of SO_2 adsorption on Saharan dust under laminar flow tube conditions.[15]

To probe the potential recovery of CO_2-forming sites on high-ordered $CaCO_3$(s), a saturated sample (Table 2, experiment 1a) was exposed to the ambient atmosphere for 5 days and subsequently exposed to SO_2 in the 14 mm orifice flow reactor. The results (Table 2, experiment 1c) are displayed in Figure 5, which reveals that the CO_2-forming ability of the previously poisoned sample returns to a certain degree. The mass balance between the loss of SO_2 and the yield of CO_2 is closed for SO_2 uptake during the first 15 min owing to the 1:1 mass balance between net SO_2 lost and CO_2 generated as for a virgin sample. The initial uptake coefficient γ_0 for the recycled sample is approximately the same as for a fresh sample. In contrast to the first uptake experiment, the sample saturates earlier, as displayed in Figure 5, and the total yield (loss) of CO_2 (SO_2) is approximately a factor of 4 lower, corresponding to 7×10^{16} molecule g^{-1} compared to the original uptake, whereas γ_0 is remarkably immune toward recycling of the $CaCO_3$(s) sample. These experiments have shown that CO_2-forming sites do not regenerate under flow reactor conditions but that they will regenerate in part under ambient conditions within a few days. In contrast, sites leading to SO_2 uptake without CO_2 formation will regenerate through pumping under flow reactor conditions, which implies the existence of a weakly bound precursor state SO_2(ads). The yield of SO_2 lost and CO_2 formed until saturation of the SO_2 uptake is significantly higher for the maiden SO_2 uptake experiment than the subsequent net loss of SO_2 on a poisoned sample. There apparently is a slow surface reaction that converts the reversibly adsorbed SO_2 into an irreversibly adsorbed state whose rate coefficient is measured as discussed below. In a further experiment the SO_2 uptake was halted before complete saturation. After a waiting period of $t_w = 5$ min, essentially no SO_2 desorbed whereas additional CO_2 was formed during the "closed" period of the experiment. This confirms the rapid rate of the CO_2-forming reaction channel that consumed SO_2(ads) as well as the small quantity of SO_2 in the closed sample compartment.

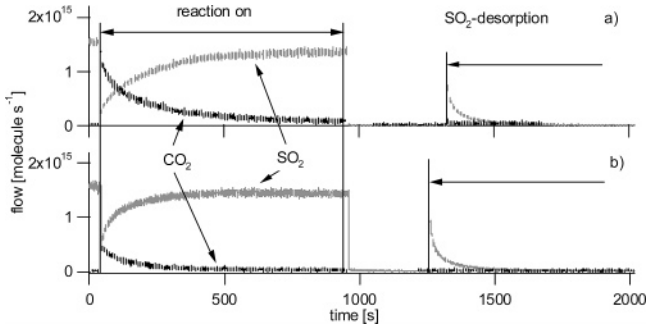

Figure 5. Uptake experiment of SO_2 on a new and used $CaCO_3$ sample. Uptake was carried out in the 14 mm orifice reactor on 1 g of precipitated high-ordered $CaCO_3$. Uptake rate of SO_2 and production rate of CO_2 on (a) a virgin $CaCO_3$(s) sample and (b) on the same sample stocked for 5 days at ambient conditions.

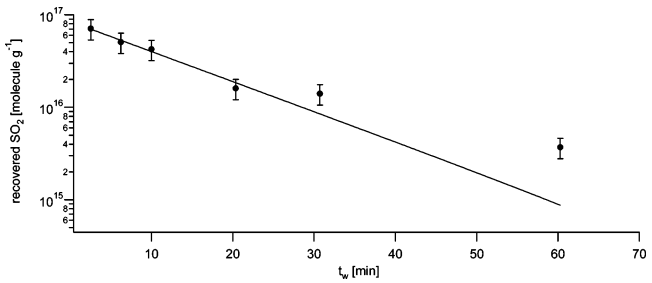

Figure 6. Amount of recovered SO_2 as a function of waiting period t_w during which the sample has been isolated from the gas flow, H_2O(ads) $= 1.1 \times 10^{18}$ molecule g^{-1}.

To express the slow net SO_2 loss, which is not measurable as an uptake of SO_2 at steady-state conditions, as a quantitative uptake, a series of SO_2 uptake experiments were performed where the reversibly adsorbed fraction of SO_2 loss was recorded as a function of t_w (Table 2, experiment 2). Figure 6 displays the results and reveals that the amount $S(t_w)$ of desorbing, that is, reversibly adsorbed, SO_2 exponentially decreases with t_w in the range from a few minutes to 60 min. The SO_2 uptake experiments did not lead to CO_2 formation, except the first one until saturation of the sample, and we conclude that reversibly adsorbed SO_2 undergoes a slow transition toward an irreversibly adsorbed state on the present time scale. Desorption of this irreversibly adsorbed SO_2 may eventually take place on a much longer time scale of hours by prolonged pumping, as indicated above. The first-order decay constant resulting from the slope of the straight line displayed in Figure 6, namely $\ln(N(t_1)/N(t_2))/$

$(t_1 - t_2)$, where $N(t)$ is the remaining or recoverable fraction of SO_2 at t, leads to $k_S = 1.2 \times 10^{-3}$ s^{-1}. The maximum recoverable amount of SO_2 $S(t=0) = 8 \times 10^{16}$ molecule g^{-1} corresponds to the extrapolated value at $t = 0$ and leads to 2.2×10^{12} molecule cm^{-2} for high-ordered $CaCO_3$(s). By comparison, the first-order rate constant k_C for the uptake of SO_2 leading to CO_2 is 10 s^{-1}, corresponding to $\gamma_0 = 0.13$ (Table 2), which is larger by 4 orders of magnitude. It appears that both processes, namely, k_C and k_S, are effectively decoupled and independent of each other.

A typical maiden SO_2 uptake experiment on high-ordered $CaCO_3$(s) (Table 2, experiment 1) leads to a yield of CO_2 and SO_2 of 2.7×10^{17} molecule g^{-1} where 8×10^{16} out of 2.7×10^{17} molecules of SO_2 (30%) are initially reversibly adsorbed. However, if the same uptake experiment is performed on low-ordered $CaCO_3$(s) under identical experimental conditions (Table 2, experiment 4) only 2 mol of CO_2 is obtained for every 3 mol of lost SO_2, leading to a change in the yield ratio SO_2-(lost)/CO_2(formed) from 1.0 to 1.5 in going from a high-ordered to a low-ordered $CaCO_3$(s) sample. Although the absolute yield of CO_2 remains the same, the relative amounts of both adsorption sites or the branching ratio between the two processes, k_C and k_S, depends on the morphology or structure of the crystalline sample.

Using the bifunctional intermediate $Ca(OH)(HCO_3)$, we propose the following competitive reaction mechanism that is consistent with all kinetic observations where SS designates an intermediate adsorption site for SO_2, that is, the gateway to adsorption on the bicarbonate or hydroxyl function:

$$SO_2(g) + SS \leftrightarrows SO_2{-}SS \tag{11}$$

$$Ca(OH)(HCO_3) + SO_2{-}SS \rightarrow Ca(OH)(HSO_3) + CO_2(g) \quad (k_C) \tag{12}$$

$$Ca(OH)(HCO_3) + SO_2{-}SS \rightarrow Ca(HSO_3)(HCO_3) \quad (k_S) \tag{13}$$

Because the ratio k_C/k_S is approximately 10^4, both reactions are effectively decoupled. In this scheme the rate-limiting reactions are either (12) or (13). However, we cannot exclude reaction 14 as a secondary reaction in competition with reaction 13 because upon initial uptake of SO_2 the high rate of reaction 12 will convert all the bicarbonate to the bisulfite species $Ca(OH)(HSO_3)$ already in the initial stages of the uptake:

$$Ca(OH)(HSO_3) + SO_2{-}SS \rightarrow Ca(HSO_3)_2 \tag{14}$$

To probe the substrate for the potential presence of $Ca(OH)_2$ on the surface SO_2, uptake experiments on solid bulk $Ca(OH)_2$ have been carried out (Table 2, experiment 3). $Ca(OH)_2$ may be formed from the precursor state according to

$$Ca(OH)(HCO_3) \leftrightarrows Ca(OH)_2 + CO_2 \tag{15}$$

The uptake of SO_2 did not saturate even under prolonged exposure and was significantly faster than for $CaCO_3$(s). No desorption of either SO_2 or other volatile products were observed at various stages of the uptake experiment. We assume that SO_2 is taken up according to

$$Ca(OH)_2 + SO_2(g) \rightarrow Ca(OH)(HSO_3) \tag{16}$$

Owing to the fast reaction of SO_2 on $Ca(OH)_2$, the saturation behavior and the absence of recoverable SO_2, we conclude that there may be only small amounts of $Ca(OH)_2$ present on the $CaCO_3$(s) sample, if any. If the SO_2 uptake reaction would occur through $Ca(OH)_2$, reaction 13 should be significantly faster and no SO_2 desorption should be observed. This essentially rules out the spontaneous conversion of $Ca(OH)(HCO_3)$ to $Ca(OH)_2$ according to reaction 15 at the present experimental conditions. In addition, no spontaneous measurable CO_2 formation was ever observed upon pumping on $CaCO_3$(s), which is evidence against reaction 15 occurring under the present experimental conditions.

Additional uptake experiments on precipitated $CaCO_3$(s) at different amounts of H_2O(ads) have been performed (Table 2, experiment 5). Two samples with H_2O(ads) of 1.1×10^{18} and 5×10^{17} molecules g^{-1} corresponding to a pumpdown time of 30 min and 21 h, respectively, have been compared. The sample with the larger amount of H_2O(ads) obtained yields 15% higher as far as integrated loss of SO_2 and yield of CO_2 has been observed, with γ_0 being higher by a factor of 2 in the sample containing more H_2O(ads). This result may be explained by the slow decrease of the number of intermediates $Ca(OH)(HCO_3)$ upon pumping according to reaction 7, as observed for CO_2. However, the influence of the pumping time on the SO_2 uptake is not very pronounced, which may be explained by the slow dehydration reaction 7 of the surface intermediate. Adams et al.[15] have also noted the absence of relative humidity effects on the SO_2 uptake on Saharan dust, which we may explain by the fact that the uptake is controlled by the number of surface intermediates that are formed by slow weathering of $CaCO_3$(s) under ambient conditions according to reaction 8. The uptake coefficient γ of SO_2 on Saharan dust was not affected by an increase in relative humidity from 0 to 27%, albeit at lower temperature (258 K). The spontaneous dehydration of the surface intermediate upon pumping following reaction 7 must be slow to explain the low sensitivity of the rate of SO_2 uptake on relative humidity in contrast to the situation for CO_2.

The present results may be compared with a recent combined FTIR spectroscopic and kinetic study by Al-Hosney et al.[7] on the heterogeneous interaction of SO_2 with calcite powder as a function of relative humidity in the range 5−95%. The saturation of calcite by SO_2 occurs at a surface concentration of 4×10^{13} molecule cm^{-2} which is a factor of 6 larger than for the present experiments. This may be explained by the higher rh values used by these authors compared to our low-pressure conditions where only a fraction of a monolayer of adsorbed water was present. However, at variance with the present experiments, these authors do not observe the formation of CO_2(g), rather they observe additional bands in the IR that they attribute to adsorbed carbonic acid, H_2CO_3, resulting from

$$Ca(OH)(HCO_3) + SO_2(g) \rightarrow CaSO_3(s) + H_2CO_3(ads) \tag{17}$$

The calcium sulfite is observable in the FTIR absorption spectrum and assigned to the formation of a crystalline sulfite. The presence of adsorbed carbonic acid is inferred by a sequence of IR absorption bands in analogy to condensed phase H_2CO_3 at 687, 839, 1022 and 1688 cm^{-1}.[40−42] Especially the intense CO stretching band at 1688 cm^{-1} is believed to be unambiguous proof for the presence of stable adsorbed carbonic acid that decomposes in the presence of adsorbed water into CO_2 and H_2O. Theoretical considerations[43] are consistent with the fast decomposition of H_2CO_3(ads) in the presence of a single nearby adsorbed water molecule. This result may be rationalized if the experiments performed by Al-Hosney et al. had been performed under "dry" conditions of extensive pumping and/or baking of the substrate. However, most experiments have been performed at significant relative humidities that imply at least fractional

TABLE 3: Typical Experimental Conditions and Main Results of HNO_3 Uptake Experiments on $CaCO_3$(s)

no.	orifice diameter (mm)	[HNO_3] (molecule cm^3)	sample[a]	experimental conditions[b]	uptake kinetics	remarks
1a	14	1.6×10^{11}	Au	bare sample holder	$\gamma_0 = 2.7 \times 10^{-3}$	saturation after a few seconds
1b	4	2.1×10^{12}	Au	bare sample holder	$\gamma_0 = 2.4 \times 10^{-4}$	saturation after a few tens of seconds
2a	14	2.7×10^{11}	pm	$t_p = 21$ h, first uptake, $t_e = 2$ min	$\gamma_0 = 1 \times 10^{-2}$	formation of H_2O
						no formation of CO_2
						loss of HNO_3: 1.4×10^{16} molecule
					$\gamma_{ss} = 2 \times 10^{-3}$	
2b	14	2.7×10^{11}	pm	$t_p = 21$ h, second uptake, $t_e = 2$ min	$\gamma_0 = 7 \times 10^{-3}$	no formation of CO_2
						no formation of H_2O
						loss of HNO_3: 4.7×10^{15} molecule
					$\gamma_{ss} = 2 \times 10^{-3}$	
2c	4	7×10^{11}	pm	$t_p = 21$ h, third uptake, $t_e = 2$ min	$\gamma_0 = 7 \times 10^{-3}$	no formation of CO_2
						no formation of H_2O
						loss of HNO_3: 1.3×10^{16} molecule
					$\gamma_{ss} = 7 \times 10^{-4}$	
2d			pm	heated at $T = 470$ K		small amounts of CO_2 observed
3a	4	5×10^{11}	cm	$t_p = 21$ h, $t_e = 3$ min	$\gamma_0 = 8 \times 10^{-2}$	formation of H_2O
						no formation of CO_2
						loss of HNO_3: 5.7×10^{16} molecule
						desorption of HNO_3: 9×10^{15}molecule
					$\gamma_{ss} = 2 \times 10^{-3}$	
4	14	$(0.2-3) \times 10^{11}$	cm	$t_p = 20$ min		γ_0 decreases and γ_{ss} does not change with concentration
5	14		p	high-ordered precipitated $CaCO_3$	$\gamma_0 = 0.3$	formation of CO_2 sets in delayed

[a] Au: gold-coated substrate. p: high-ordered precipitated $CaCO_3$. pm: polished marble. cm: cut marble. [b] t_p: pumping time. t_e: exposure time.

monolayers of adsorbed water on the calcite substrate. It is possible that adsorbed H_2CO_3 is also formed under our experimental conditions of essentially zero rh but known amounts of adsorbed H_2O. However, at least on high-ordered calcite the yield of H_2CO_3(ads) cannot be significant owing to the closed mass balance between adsorbed SO_2 and generated CO_2 as discussed above. Therefore, it is not clear at present how to resolve the apparent contradiction under the relative circumstances of both experiments: on one hand the experimental conditions of the present experiments lead to small but measurable amounts of adsorbed H_2O as displayed in Figure 1, but no significant amounts of products other than CO_2(g). On the other hand, the high humidity conditions of Al-Hosney et al.[7] seem to support adsorbed H_2CO_3 despite its expected instability with respect to decomposition to H_2O and CO_2.[43]

In conclusion, SO_2 preferentially attacks the bicarbonate group of the bifunctional surface intermediate Ca(OH)(HCO_3) whereas the OH group reacts at a much slower rate. It seems that, similarly to the case for CO_2, the uptake of SO_2 is controlled by the abundance of available bifunctional surface intermediate Ca(OH)(HCO_3) at the gas−solid interface.

Adsorption of HNO_3. As discussed above, the kinetics of the HNO_3 uptake on $CaCO_3$(s) has been studied recently on numerous occasions in the context of using calcite as a surrogate substrate for atmospheric mineral dust.[7,19−24,44] This work is focused on mechanistic aspects whose goal is to understand the role of the postulated bifunctional intermediate Ca(OH)(HCO_3) in its interaction with key atmospheric trace gases. HNO_3 is a "sticky" gas whose complexities in handling in laboratory investigations has often been overlooked. Therefore, HNO_3 reference experiments on the bare gold-coated sample holder have been performed. A small rate of uptake that saturates after a few seconds corresponding to $\gamma_0 = 2.7 \times 10^{-3}$ and 2.4×10^{-3} in the 14 and 4 mm orifice reactor, respectively, have been measured (Table 3, experiments 1a and 1b). This contribution has been subtracted from the sample runs knowing that it represents an upper limit because the sample covers a fraction of the Au-coated sample holder thus diminishing the contribution of HNO_3 taken up by the bare sample support.

Because HNO_3 uptake on powdered calcite has been studied extensively in the past using the same technique[19,20,22] the emphasis in the present study is placed on HNO_3 uptake experiments on marble disks to obtain additional insight into the uptake mechanism. These uptake experiments on a polished marble disk carried out in the 14 mm orifice reactor have revealed an apparent saturation of the uptake rate after 2 min or so at a flow rate $F^{in} = 5.5 \times 10^{14}$ molecule s^{-1} of HNO_3 into the reactor resulting in HNO_3 concentrations displayed in Table 3 (experiments 2a and 2b). In contrast to the heterogeneous interaction of HNO_3 on $CaCO_3$(s) powder, no CO_2 formation was observed whereas a measurable H_2O rate of formation could be measured. Care was taken to measure the HNO_3 uptake on a sample that was always pumped for the same length of time compared to the measurement of H_2O(ads) in the absence of HNO_3 to obtain identical conditions for the H_2O reference and the HNO_3 uptake experiment. The net H_2O production rate was obtained by subtraction of the total at HNO_3 exposure minus the reference MS signal at identical H_2O(ads). The mass balance of the total yield of generated H_2O vs loss of HNO_3 by uptake, typically 3.8×10^{14} vs 5.0×10^{14} molecule cm^{-2} using the geometric surface area of 27.4 cm^2, suggests a 1:1 correspondence between the loss of HNO_3 vs formation of H_2O.

The estimated surface density of $CaCO_3$ ion pairs is 6.7×10^{14} molecule cm^{-2} so that approximately 50% of a formal monolayer of $CaCO_3$(s) contributes to reactive uptake of HNO_3 on a polished marble substrate within 2 min or so. A similar uptake experiment carried out in the 4 mm orifice reactor on an identical substrate has shown uptake of HNO_3 but formation of neither H_2O nor CO_2 within the present detection limits (Table 3, experiment 2c). Thermal desorption of a saturated polished marble disk at $T = 470$ K revealed small amounts of CO_2 but no HNO_3 (Table 3, experiment 2d).

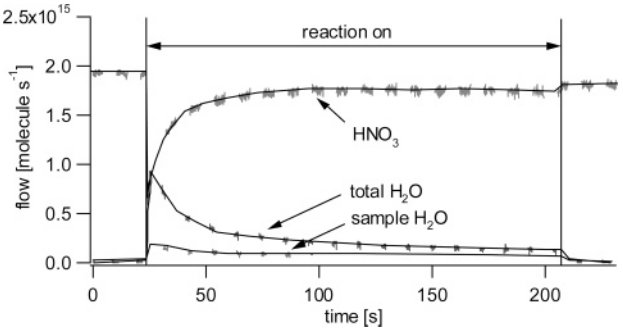

Figure 7. HNO_3 uptake experiments performed on a cut $CaCO_3$ marble disk in the 14 mm orifice reactor. The sample flow of H_2O is the difference between the total and the flow from the marble sample in the absence of HNO_3 and corresponds to the product of the heterogeneous reaction.

Additional HNO_3 uptake experiments have been performed on cut marble disks of which a typical result is displayed in Figure 7. It shows an experiment using the 14 mm orifice reactor that leads to a rapid initial HNO_3 uptake tending toward steady state at $t = 200$ s, which is accompanied by a corresponding H_2O rate of formation in the absence of detectable CO_2 (Table 3, experiment 3a). As for the case of polished marble, we observe quantitative agreement between HNO_3 consumed and H_2O formed on the $CaCO_3$(s) substrate, which suggests that HNO_3 uptake initially occurs according to reaction 18 without the formation of CO_2. These results obtained on low surface

$$Ca(OH)(HCO_3) + HNO_3(g) \rightarrow Ca(NO_3)(HCO_3) + H_2O \quad (18)$$

area substrates such as polished and cut marble substrates emphasize the initial phase of HNO_3 uptake in contrast to large surface area $CaCO_3$(s) substrates discussed below. They represent proof of the reactivity of the OH group of the surface intermediate in reactive uptakes. Qualitatively, we note an increase of γ_0 from 1×10^{-2} to 4×10^{-2} in going from the polished to the cut, that is, rough, $CaCO_3$(s) substrate surface. There is also an increase in the amount of HNO_3 taken up by a factor of 4 resulting in 1.2×10^{15} molecule cm^{-2} of HNO_3 taken up on a cut marble disk. This confirms the presence of additional reactive sites on a cut compared to a polished $CaCO_3$-(s) substrate.

Significant amounts of HNO_3 have been observed desorbing from a cut marble substrate after exposure to HNO_3 for 15 min at $F^{in} = 4 \times 10^{14}$ molecule s^{-1} in the 4 mm orifice reactor once the inflow of HNO_3 had been halted. A yield of typically 20% of recovered HNO_3 compared to HNO_3 lost upon adsorption has been measured. This desorption of HNO_3 after halting the inflow suggests the presence of surface sites that may adsorb HNO_3 on the substrate before undergoing a chemical conversion according to reaction 18. Reaction 19 describes the formation of a weakly, presumably H-bonded precursor state prior to reaction. Figure 8 displays $\gamma(t)$ of HNO_3 interacting with cut

$$HNO_3(g) + SS \leftrightarrows HNO_3{-}SS \quad (19)$$

marble plates carried out in the 14 mm orifice reactor at three different HNO_3 concentrations (Table 3, experiment 4). A sample exposed to a high $[HNO_3]$ saturates faster than one exposed to a lower one whereas all γ values seem to tend toward the same steady-state γ values at a reaction time of 6 min or longer. However, γ_0 decreases with increasing $[HNO_3]$ probably owing to saturation of the limited amount of surface sites. This result represents additional proof for the finite number of

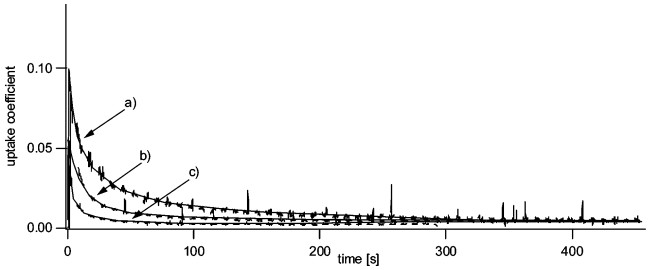

Figure 8. Uptake coefficient $\gamma(t)$ of HNO_3 as a function of reaction time carried out in the 14 mm orifice reactor on cut marble plates. $[HNO_3]$ is (a) 2.8×10^{10}, (b) 8.5×10^{10}, and (c) 2.8×10^{11} molecule cm^{-3}.

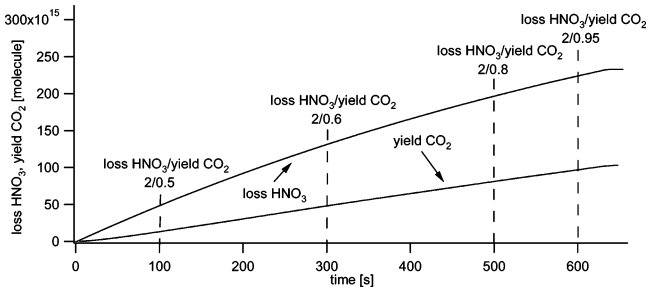

Figure 9. Yield of HNO_3 lost (upper) and CO_2 generated (lower curve) during a typical uptake experiment of HNO_3 on 1 g of high-ordered precipitated $CaCO_3$(s) measured in the 14 mm orifice reactor. Selected ratios of both yields are displayed as a function of time.

reactive sites on the $CaCO_3$(s) substrate. To investigate a saturated cut marble substrate for its capacity for regeneration, it was isolated from the gas flow for 15 min after saturation. No additional uptake of HNO_3 was observed, which means that the poisoned $CaCO_3$(s) sample does not regenerate its activity under flow reactor conditions unlike SO_2 uptake. In the presence of high relative humidity leading to appreciable quantities of mobile adsorbed H_2O(ads) atop the calcite surface the reaction mechanism is expected to change according to reactions 2 and 3 that are known to proceed rapidly in aqueous solution. We surmise that the dissolution of calcite or of any carbonate in acidic aqueous solution does not necessarily require the bifunctional surface intermediate invoked in the interfacial reaction of acidic trace gases with calcite at low abundance of H_2O(ads). The corollary of the present study is that the bifunctional surface intermediate and the mobile adlayer of adsorbed H_2O may each support different mechanisms of carbonate corrosion by atmospheric trace gases depending on relative humidity.

Typical results of HNO_3 uptake on precipitated high-ordered $CaCO_3$(s) samples presented as a powder are displayed in Table 3, experiment 5. This uptake experiment carried out in the 14 mm orifice reactor is characterized by large values of γ_0, on the order of 0.3 and by the delayed formation of CO_2, as has been observed by Fenter et al..[19] Because of the large amount of H_2O vapor desorbing from the powder sample it has not been possible to unambiguously monitor the H_2O formed in reaction 18 as was the case for the marble disks. Figure 9 displays the yield of both HNO_3 lost and CO_2 formed, which shows the delay of CO_2 formation with respect to the instant onset of HNO_3 formation. The resulting yield of HNO_3 lost amounted to 4.8×10^{17} molecule g^{-1} when the decreasing rate of HNO_3 formation was extrapolated to zero (not shown) and is in good agreement with twice the yield of CO_2, namely, 2.7×10^{17} molecule g^{-1}, resulting from the uptake of SO_2 on the same type of precipitated $CaCO_3$(s) performed at the same experimental conditions (Table 2, experiment 1a). The total CO_2 yield

TABLE 4: Typical Experimental Conditions and Main Results of HCl Uptake Experiments on $CaCO_3$(s)

no.	orifice diameter (mm)	[HCl_3] (molecule cm^3)	sample[a]	experimental conditions	uptake kinetics	remarks
1a	14	6×10^{11}	p	estimated H_2O(a): 5×10^{18} molecule g^{-1}, first uptake	$\gamma_0 = 0.13$	formation of CO_2 is delayed no formation of gaseous H_2O measured
1b	14	6×10^{11}	p	third uptake experiment	$\gamma_0 = 6 \times 10^{-2}$	formation of CO_2, loss rate of HCl/rate of formation of CO_2 tends toward 2
2	4	5×10^{12}	p	desorption from a sample previously exposed to HCl		desorption of HCl and of small amounts CO_2
3	14					
4	14	6×10^{12}	p	estimated H_2O(a): 5×10^{18} molecule g^{-1}	$\gamma_0 = 0.13$	uptake of H_2O $\gamma(H_2O) = 7 \times 10^{-2}$
5	1	1×10^{14}	cm		$\gamma = 3 \times 10^{-4}$	no reaction products observed

[a] cm: cut marble. p: high-ordered precipitated $CaCO_3$.

was assumed to be equal to the number of available reactive surface sites Ca(OH)(HCO_3), and from the above yield ratio 2 mol of HNO_3 will react per mole of surface intermediate thereby releasing one mole of CO_2. The following reaction mechanism for the heterogeneous reaction of HNO_3 with precipitated $CaCO_3$(s) is consistent with the present experimental results:

$$HNO_3(g) + SS \leftrightarrows HNO_3{-}SS \quad (20)$$

$$Ca(OH)(HCO_3) + HNO_3{-}SS \rightarrow Ca(NO_3)(HCO_3) + H_2O \quad (18a)$$

$$Ca(NO_3)(HCO_3) + HNO_3{-}SS \rightarrow Ca(NO_3)_2 + CO_2 \quad (21)$$

The reaction mechanism explains the delay in the CO_2 formation and the formation of H_2O highlighted in the experiments with marble disks. The absence of CO_2 as a reaction product for the marble substrate may be a consequence of the small number of available surface intermediates and/or because reaction 21 may be rate-limiting, that is, slow, compared to reaction 20.

In analogy to the heterogeneous reaction of SO_2 with calcite, Al-Hosney et al. [7] studied the reaction of HNO_3 with calcite powder using FTIR absorption spectroscopy at relative humidities in the range 5−95%. Both calcium nitrate and adsorbed carbonic acid H_2CO_3(ads), but no CO_2(g), have been observed as in the case of SO_2. Saturation of the calcite substrate occurred after 2.7×10^{14} HNO_3 molecules cm^{-2} had been adsorbed whereas 1.3×10^{13} molecules cm^{-2} already was sufficient for saturation in the present study. This disagreement may perhaps be attributed to differences in relative humidities in both studies. Here, as in the case of SO_2 outlined above, the present results do not leave room for significant amounts of a product at long reaction times, other than CO_2(g), in view of the closed mass balance between HNO_3 lost and CO_2 generated within experimental uncertainty.

However, as illustrated in Figure 9 the 2:1 mass balance between HNO_3 lost and CO_2 formed is attained only at long reaction times, as there is a noticeable delay in CO_2 formation compared to HNO_3 loss as has been pointed out by Fenter et al..[19] Figure 9 displays mass balance ratios of HNO_3 lost to CO_2 formed of 4:1, 3:1, 2.5:1 and 2.15:1 at 100, 300, 500 and 600 s of interaction time, respectively. It is obvious that the mass balance tends toward 2:1 at long reaction times. Therefore, it may be possible that some of the missing CO_2(g) may be sequestered as H_2CO_3(ads) at short reaction times. However, the only way to reconcile the absence of H_2CO_3(ads) in the present study would be to postulate that the present experiments were performed under "humid"conditions that would lead to destruction of carbonic acid, hence to CO_2(g), whereas the experiments performed by Al-Hosney et al. would have been performed under "dry"conditions, a contradiction with respect to the chosen conditions of both studies as already pointed out for SO_2. The appropriate label for the present experiment and for Al-Hosney et al. are "dry" and "humid", respectively, in terms of relative humidity. However, an alternative way of reconciling both experiments would be to reassign the IR bands attributed by Al-Hosney et al. to H_2CO_3(ads) instead to Ca(HSO_3)(HCO_3) and Ca(NO_3)(HCO_3) for the adsorption of SO_2 and HNO_3, respectively. In this case the IR bands would be characteristic of a bicarbonate-containing surface intermediate that is expected to be more stable than H_2CO_3(ads). This reassignment would make the results consistent with each other if one would assume that the evolving CO_2 in the case of the SO_2 attack (see above) on Ca(OH)(HCO_3) would react with the OH group of the intermediate Ca(OH)(HSO_3) akin to reaction 10 to result in Ca(HSO_3)(HCO_3) to explain the absence of CO_2 in the experiments of Al-Hosney et al..[7]

In conclusion, HNO_3 first attacks the OH group of the bifunctional surface intermediate, followed by the bicarbonate group that releases CO_2 after some time delay in contrast to SO_2 uptake that follows the inverse sequence. It appears that the kinetics of heterogeneous reaction of gas-phase HNO_3 on precipitated $CaCO_3$(s) depends on the abundance of available bifunctional surface intermediates because HNO_3 uptake becomes immeasurable at steady-state. Saturation was observed on marble disks that presented a limited number of surface intermediates compared to calcite powder.

Adsorption of HCl. Uptake experiments of HCl have been performed on high-ordered $CaCO_3$(s) in the 14 mm orifice reactor. Despite the high-order substrate that is associated with a low density of (reactive) defect sites, the reactivity is quite high as may be viewed in Table 4, experiment 1a and Figure 10. The only observed reaction product was CO_2 whose

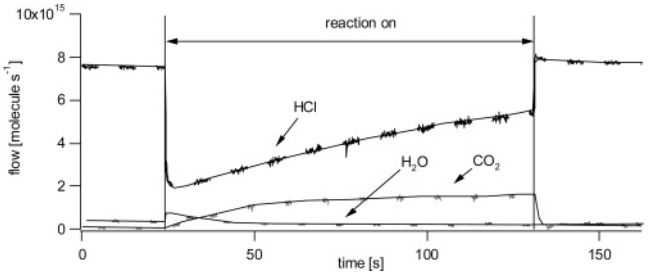

Figure 10. Typical HCl uptake experiment on 1 g of high-ordered precipitated $CaCO_3$ carried out in the 14 mm orifice reactor. HCl, H_2O and CO_2 have been monitored at $m/e = 36$, $m/e = 18$ and $m/e = 44$, respectively.

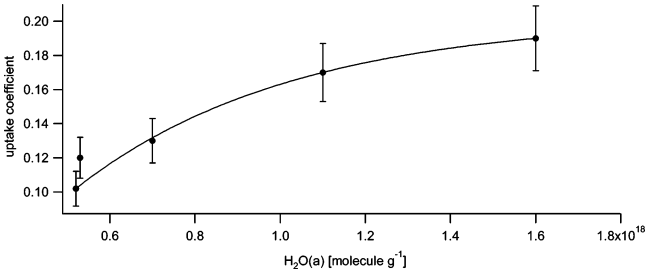

Figure 11. HCl uptake experiments on 1 g of high-ordered precipitated $CaCO_3$ carried out in the 14 mm orifice reactor at [HCl] = 6×10^{11} molecule cm^{-3}. The graph shows the initial uptake coefficient based on the geometrical area of the sample as a function of H_2O(ads) evaluated using the calibration curve of Figure 1.

formation sets in with a time delay similar to that for HNO_3 uptake experiments on precipitated $CaCO_3$(s). However, in contrast to these no formation of gaseous H_2O has been observed. The uptake experiment displayed in Figure 10 displays a partial saturation whereas subsequent HCl uptake experiments performed on the same substrate led to steady-state uptake. To compare the loss of HCl with the yield of CO_2, both loss of HCl and formation of CO_2 have been integrated over all performed HCl uptake experiments carried out on the sample whose maiden uptake experiment is shown in Figure 10. On average, a total loss of 8.8×10^{17} molecules of HCl g^{-1} has been recorded in conjunction with a total yield of 4.1×10^{17} molecules g^{-1} of CO_2. This means that 2 mol of HCl is converted into 1 mol of CO_2.

After lowering the isolation plunger and halting the HCl flow, we open the sample compartment again. HCl desorption was observed in an experiment whose details are listed in Table 4, experiment 2. Similar to the situation for HNO_3, the desorption of HCl points toward the existence of a weakly bound HCl precursor that reacts further in a rate-limiting step following

$$\mathrm{HCl} + \mathrm{SS} \leftrightarrows \mathrm{HCl{-}SS} \qquad (22)$$

The effect of H_2O(ads) on the kinetics of HCl adsorption was investigated by comparing two HCl uptakes at 5×10^{17} and 1.6×10^{18} H_2O(ads) g^{-1} of at [HCl] = 6×10^{11} molecule cm^{-3} in the 14 mm orifice reactor. Two results may be stated, namely that γ_0 increases somewhat with H_2O(ads) similarly to that for CO_2 and that the delay time for CO_2 formation decreases with H_2O(ads). Figure 11 displays γ_0 as a function of H_2O(ads) at conditions detailed in Table 4, experiment 3. It increases from $\gamma_0 = 0.1$ to 0.19 over the indicated range of H_2O(ads), which corresponds to the same increase by a factor of roughly 2 as was the case in the $SO_2/CaCO_3$(s) system presented above, which shows the importance of residual water in the reaction mechanism. When all kinetic observations are put together, the following reaction mechanism involving the bifunctional reactive surface intermediate expressed in reactions 22−24 may be formulated. With decreasing amounts of H_2O(ads) owing to

$$\mathrm{HCl} + \mathrm{SS} \leftrightarrows \mathrm{HCl{-}SS} \qquad (22)$$

$$\mathrm{Ca(OH)(HCO_3)} + \mathrm{HCl{-}SS} \rightarrow \mathrm{CaCl(HCO_3)} + \mathrm{H_2O(ads)} \qquad (23)$$

$$\mathrm{CaCl(HCO_3)} + \mathrm{HCl{-}SS} \rightarrow \mathrm{CaCl_2} + \mathrm{CO_2} + \mathrm{H_2O(ads)} \qquad (24)$$

prolonged pumping equilibrium (7) is shifted toward the formation of bulk unreactive $CaCO_3$(s) at the expense of the amount of the reactive bifunctional surface intermediate, which will lead to a smaller rate of uptake of HCl and a delay of CO_2 formation in reaction 24.

TABLE 5: Summary of the Initial Uptake Coefficients γ_0 of Trace Gases on $CaCO_3$

trace gas species	substrate	H_2O(ads) (molecule g^{-1})	this work	lit.
CO_2	precipitated $CaCO_3$	$<2 \times 10^{18}$	$<2 \times 10^{-4}$	
SO_2	precipitated $CaCO_3$	1×10^{18}	0.1	
HNO_3	precipitated $CaCO_3$		0.29	
	polished marble		1×10^{-2}	
	cut marble		4×10^{-2}	
	$CaCO_3$ powder			0.1[19]
				0.1[20]
				2.5×10^{-4} [22]
HCl		5×10^{18}	0.13	

According to reactions 23 and 24 one expects 2 mol of H_2O for 2 mol of HCl lost to the surface of $CaCO_3$(s); however, no water vapor in excess to H_2O(ads) has been found at the present experimental conditions. This result is in stark contrast to HNO_3 uptake experiments on the same substrate presented above. When the MS signal at *m*/*e* 18 is recorded at the start of the uptake experiment in the 14 mm orifice reactor, it gradually decreases by almost a factor of 2 and returns to background level once the $CaCO_3$(s) substrate is isolated from the gas flow. The details may be found in Table 4, experiment 4. We expect the final reaction product to be $CaCl_2$, which is known to be a highly hygroscopic species. We assume that the formation of 1 mol of $CaCl_2$ binds 2 mol of H_2O according to

$$\mathrm{CaCl_2} + 2\mathrm{H_2O(ads)} \rightarrow \mathrm{CaCl_2 \cdot 2H_2O(s)} \qquad (25)$$

The formation of a crystalline complex of $CaCl_2$, containing 2 mol of H_2O,[45] would explain the absence of H_2O in the gas phase despite it being a primary reaction product.

HCl uptake experiments on polished marble have led neither to a measurable rate of uptake nor to reaction products; however, uptake on cut marble disks have led to a slow uptake of HCl but to no detectable reaction products. Owing to the low values of the uptake coefficient the experiment was performed in the 1 mm orifice reactor whose details may be found in Table 4, experiment 5. The absence of a significant HCl uptake on marble disks underlines the importance of the abundance of the bifunctional reactive surface intermediates that depends on the surface and structural properties of the $CaCO_3$(s) substrate. We assume that the number of surface defects as well as the presence of H_2O and CO_2 at ambient conditions strongly favor the formation of the surface intermediate according to reaction 8.

Comparison of the Initial Uptake Coefficient γ_0 with Literature Results. Table 5 displays a summary of the uptake coefficients γ_0 obtained in this work and from the literature where we strictly limit our comparison to calcite. For the interaction of CO_2, SO_2 and HCl the present work is the first to report quantitative results whereas there are three previous studies on HNO_3/calcite.[19,20,22] The agreement between the present results and Fenter et al.[19] is satisfactory in view of the difference between the calcite samples used in both studies. In addition, we would like to point out that Fenter et al. have measured $\gamma = (5 \pm 2) \times 10^{-2}$ for the uptake of H_2O on milled (ground) calcite powder whereas we have been unable to measure the kinetics of H_2O uptake on calcite used in the present study. The probable reason lies in the fact that γ is immeasurably small for the high- and low-ordered $CaCO_3$ samples used in this study. This therefore emphasizes the importance of sample characterization and control.

Hanisch and Crowley[20] report $\gamma_0 = (1 \pm 0.25) \times 10^{-1}$ and $(1.8 \pm 0.45) \times 10^{-1}$ on heated (363 K) and unheated $CaCO_3$,

respectively, which is in excellent agreement with the present study. These workers advance arguments, both experimental and theoretical, in favor of taking the geometric surface area for the calculation of the numerical value of γ_0 in complete agreement with the present work. Similarly to the present study, they also report CO_2 and H_2O as primary products of the heterogeneous interaction, albeit to a variable extent. For humid and dry $CaCO_3$ powder they report 2.7 and 3.4 HNO_3 taken up per CO_2 generated on the time scale of their uptake experiment whereas we report a limiting yield ratio of 2.0 based on results displayed in Figure 9 that is expected according to the stoichiometry (reactions 18 and 21). Hanisch and Crowley[20] report $\gamma_0 = (1.75 \pm 0.39) \times 10^{-3}$ and $(9.6 \pm 1.2) \times 10^{-4}$ for the uptake of HNO_3 on unpolished and polished $CaCO_3$ (104) single-crystal surfaces, which is an unmistaken sign that the uptake kinetics of HNO_3 on $CaCO_3$ depends on crystal imperfections of the crystalline substrate that act as surface sites in the presence of H_2O(ads).

In contrast, Underwood et al.[22] report a "true value" $\gamma_0 = (2.5 \pm 0.1) \times 10^{-4}$ after pore diffusion correction based on a measured value on the order of $\gamma_0 = 3.2 \times 10^{-2}$, which is approximately up to a factor of 10 lower than the value obtained in this work. There are two likely reasons for this significant disagreement: for one, Underwood et al. have performed their uptake experiment using residual mass spectrometry that includes the response of the detection chamber to the presence of HNO_3. It is a well, but perhaps not widely known, fact that due care has to be exercised when very sticky molecules such as HNO_3 are used in flow reactors. For these cases molecular beam sampling mass spectrometry is mandatory, as has been repeatedly shown in the past because residual MS as a detection method only works well in certain cases.[46] The factor of 2 uncertainty in γ_0 given by Underwood et al.[22] in relation to adsorption and desorption of HNO_3 on the Teflon-coated walls of the reaction vessel upon uptake turns out to be far too optimistic and leads to uncertainties of at least an order of magnitude in γ_0, especially in view of the fact that Underwood et al. use typical HNO_3 concentrations that are larger by a factor of 50 compared to the present study. In addition, we have advanced arguments in the past according to which it is inappropriate to apply the pore diffusion correction for highly sticky molecules such as HNO_3[47] because Knudsen diffusion into the bulk of the powder is slower by at least a factor of several 100 compared to a nonsticky or noninteracting molecule of the same mass. In conclusion, to obtain accurate γ_0 values for HNO_3 uptake molecular beam sampling MS as well as corrections due to adsorption/desorption processes of HNO_3 on the Teflon-coated vessel walls are mandatory in conjunction with the requirement of working at very small HNO_3 concentrations. Aguzzi and Rossi have shown a possible way of correcting γ_0 for the change of the HNO_3 coverage on the vessel walls in conjunction with performing uptake measurements using HNO_3 on ice.[48]

Conclusions

The present experiments have been performed on calcite, whose adsorbed water content H_2O(ads) corresponded to a fraction of a formal monolayer that was distributed between strongly and weakly bound H_2O in the range 1.35−5.5% of a formal monolayer, respectively, depending on the pumping time and thermal treatment of the calcite sample. In contrast, the adsorbed water content at 33% rh and ambient temperature corresponds to a total of 3.5 formal monolayers that form a mobile adsorbed layer of water beyond the first monolayer of H_2O(ads). Therefore, the present low-pressure study emphasizes the reactivity of a bifunctional surface intermediate, Ca(OH)-(HCO_3), with the gas phase as opposed to reactions of the mobile liquid phase interacting with bulk $CaCO_3$ that resemble liquid-like reactions. All obtained kinetic results are consistent with the presence of this bifunctional surface intermediate whose reactivity with the four investigated atmospherically relevant gases is schematically displayed in Figure 12 as bulk $CaCO_3$ seems to be unreactive by itself under the present experimental conditions. Under the present low-pressure conditions the rate of the heterogeneous interaction of trace gases with calcite is controlled by the number of available bifunctional surface intermediates that are created by slow weathering processes in reaction 8. Depending on the gas, either the OH or the bicarbonate group may react once a weakly bound precursor X-SS is formed on the surface, where X is the trace gas and SS is an active adsorption site.

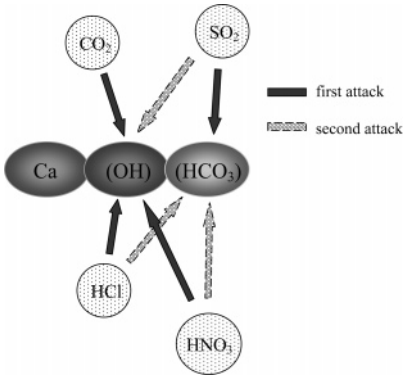

Figure 12. Synopsis of reactivity of the four trace gases CO_2, SO_2, HNO_3 and HCl with precipitated $CaCO_3$(s) via the bifunctional surface intermediate $Ca(OH)(HCO_3)$.

The uptake of CO_2 on calcite strongly depends on the partial pressure of both CO_2 (P_{CO_2}) and H_2O(ads) and may be expressed by an equilibrium constant $\kappa = \Delta CO_2/(H_2O(ads)\,[CO_2]) = 1.62 \times 10^3$ bar^{-1}. In addition, the initial uptake coefficient γ_0 being in the 10^{-4} range also scales with H_2O(ads). CO_2 interacts with calcite by specifically adsorbing on active sites of the type of the bifunctional surface adsorbate most probably resulting in surface bicarbonate. CO_2 is therefore a molecular probe for basic surface hydroxyl groups.

In contrast to CO_2 the yield of SO_2 taken up on calcite is rather insensitive to the quantity of H_2O(ads). However, γ_0 roughly scales with H_2O(ads) as is the case for HNO_3 and HCl. Similar to the case for CO_2, it was shown that the interaction of SO_2 with calcite cannot be understood on the basis of Henry's law and the quantity of H_2O(ads). As displayed in Figure 12, the primary reaction of SO_2 occurs on the HCO_3 group through rapid formation of a weakly bound SO_2-calcite precursor that subsequently reacts on a slower time scale and releases CO_2. In contrast, the reaction with OH results in bisulfite in a concurrent reaction taking place on a much slower time scale of tens of minutes with a first-order rate constant $k = 1.2 \times 10^{-3}$ s^{-1}. The initial value of γ_0 lies between 0.1 and 0.2 where up to 30% of initially adsorbed SO_2 may desorb again upon pumping at ambient temperature.

Uptake of HNO_3 on low surface area calcite, namely marble, has shown exclusive formation of H_2O in contrast to calcite powder that showed formation of both H_2O and CO_2. The uptake mechanism involves the primary reaction of HNO_3 with the hydroxyl moiety of the bifunctional intermediate, as displayed in Figure 12. The delayed formation of CO_2 for HNO_3 uptake on calcite powder and desorption of HNO_3 from exposed marble

samples are consistent with fast formation of a weakly bound precursor and rate-controlling generation of H_2O and still slower release of CO_2 resulting in $Ca(NO_3)_2$ as 2 mol of HNO_3 is consumed for every mole of CO_2 generated. The marble is a good example for the importance of sample presentation that controls the abundance of reactive adsorption sites in terms of the bifunctional surface intermediate which is reflected in low values of γ_0 on the order of 10^{-3} to 10^{-2}. The uptake of HCl on $CaCO_3$ of different morphology (cut, polished marble, high-ordered, low-ordered precipitated $CaCO_3$) leads to a mechanism identical to that for HNO_3 except that no H_2O has been observed in the gas phase. This result is explained by the fact that the solid reaction product $CaCl_2$ crystallizes as a dihydrate whose stability is consistent with the hygroscopic behavior of $CaCl_2$. In contrast to that for HNO_3, γ_0 of HCl depends on the abundance of H_2O(ads) but is similar in magnitude to that for HNO_3.

We expect that under atmospheric conditions the importance of the bifunctional surface intermediate is lessened in favor of a liquidlike reaction mechanism involving the adsorbed mobile aqueous layer at atmospheric humidities. This aqueous layer supports an acid-catalyzed ionic mechanism that is operating in the dissolution of calcite in aqueous solution.

Acknowledgment. We gratefully acknowledge generous funding of this work by the Office Fédéral de l'enseignement et de la science (OFES). This research was performed within the subproject MINATROC which is a part of the fifth framework program (FWPV) on Environment and Climate supported by the European Union (EU).

Supporting Information Available: MS signal of CO_2 uptake. This material is available free of charge via the Internet at http://pubs.acs.org.

References and Notes

(1) Loyepilot, M. D.; Martin, J. M.; Morelli, J. *Nature* **1986**, *321*, 427−428.

(2) Tabazadeh, A.; Jacobson, M. Z.; Singh, H. B.; Toon, O. B.; Lin, J. S.; Chatfield, R. B.; Thakur, A. N.; Talbot, R. W.; Dibb, J. E. *Geophys. Res. Lett*. **1998**, *25*, 4185.

(3) Stipp, S. L. S.; Eggleston, C. M.; Nielsen, B. S. *Geochim. Cosmochim. Acta* **1994**, *58*, 3023−3033.

(4) Stipp, S. L. S. *Geochim. Cosmochim. Acta* **1999**, *63*, 3121−3131.

(5) De Leuuw, N. H.; Parker, S. C. *J. Phys. Chem. B* **1998**, *102*, 2914−2922.

(6) Kendall, T. A.; Martin, S. T. *Geochim. Cosmochim. Acta* **2005**, *69*, 3257−3263.

(7) Al-Hosney, H. A.; Grassian, V. H. *Phys. Chem. Chem. Phys.* **2005**, *7*, 1266−1276.

(8) Gombert, P. *Global Planetary Change* **2002**, *33*, 177−184.

(9) Graedel, T. E. *J. Electrochem. Soc*. **2000**, *147*, 1006−1009.

(10) Plummer, L. N.; Wigley, T. M. L.; Parkhurst, D. L. *Am. J. Sci*. **1978**, *278*, 179−216.

(11) Gabrovsek, F.; Dreybrodt, W. *Water Resources Res.* **2000**, *36*, 1179−1188.

(12) Dentener, F. J.; Carmichael, G. R.; Thang, Y.; Lelieveld, J.; Crutzen, P. J. *Geophys. Res. A* **1996**, *101*, 22869−22889.

(13) Graedel, T. E.; Keene, W. C. *Global Biochem. Cycles* **1995**, *9*, 47−77.

(14) Archuleta, C. M.; Demott, P. J.; Kreidenweis, S. M. *Atmos. Chem. Phys.* **2005**, *5*, 2617−2634.

(15) Adams, J. W.; Rodriguez, D.; Cox, R. A. *Atmos. Chem. Phys.* **2005**, *5*, 2679−2689.

(16) Usher, C. R.; Al-Hosney, H.; Carlos-Cuellar, S.; Grassian, V. H. J. Geophys. Res. 107, no. D23, 4713, doi: 10.1029/2002JD002051.

(17) Ullerstam, M.; Vogt, R.; Langer, S.; Ljungstöm, E. *Phys. Chem. Chem. Phys.* **2002**, *4*, 4694−4699.

(18) Ullerstam, M.; Johnson, M. S.; Vogt, R.; Ljungström, E. *Atmos. Chem. Phys.* **2003**, *3*, 2043−2051.

(19) Fenter, F. F.; Caloz, F.; Rossi, M. J. *Atmos. Environ.* **1995**, *29*, 3365−3372.

(20) Hanisch, F.; Crowley, J. N. *J. Phys. Chem. A* **2001**, *105*, 3096−3106.

(21) Hanisch, F.; Crowley, J. N. *Phys. Chem. Chem. Phys*. **2001**, *3*, 2474−2482.

(22) Goodman, A. L.; Underwood, G. M.; Grassian, V. H. *J. Geophys. Res.* **2000**, *105*, 29053−29064.

(23) Underwood, G. M.; Li, P.; Al-Abadleh, H.; Grassian, V. H. *J. Phys. Chem.* **2001**, *105A*, 6609−6620.

(24) Seisel, S.; Börensen, C.; Vogt, R.; Zellner, R. *Phys. Chem. Chem. Phys.* **2004**, *6*, 5498−5508.

(25) Seisel, S.; Lian, Y.; Keil, Th.; Trukhin, M.; Zellner, R. *Phys. Chem. Chem. Phys.* **2004**, *6*, 1926−1932.

(26) Gustafsson, R. J.; Orlov, A.; Badger, C. L.; Griffiths, P. T.; Cox, R. A.; Lambert, R. M. *Atmos. Chem. Phys. Discuss.* **2005**, *5*, 7191−7210.

(27) Golden, D. M.; Spokes, G. N.; Benson, S. W. *Angew. Chem. IE* **1973**, *12*, 534−546.

(28) Caloz, F.; Fenter, F. F.; Tabor, K. D.; Rossi, M. *J. Rev. Sci. Instrum.* **1997**, *68*, 3172−3179.

(29) Lowell, S. *Introduction to Powder Surface Area*; John Wiley and Sons: New York, 1979.

(30) de Leuuw, N. H.; Parker, S. C. *J. Chem. Soc., Faraday Trans. 1* **1997**, *93*, 467−475.

(31) Wright, W.; Cygan, R. T.; Slater, B. *Phys. Chem. Chem. Phys.* **2001**, *3*, 839−844.

(32) Liang, Y.; Lea, A. S.; Baer, D. R.; Engelhard, M. H. *Surf. Sci.* **1996**, *351*, 172.

(33) Chiarello, R. P.; Roy, A. W.; Sturchio, N. C. *Geochim. Cosmochim. Acta* **1993**, *57*, 4103.

(34) Baedecker, P. A.; Reddy, M. M. *J. Chem. Educ*. **1993**, *70*, 104−108.

(35) Krauskopf, K. B.; Bird, B. K. *Introduction to Geochemistry*; MacGraw Hill 1995; p 647.

(36) Lasaga, A. C. *Kinetic Theory in Earth Science*; Princeton University Press: Princeton, NJ, 1998; p 811.

(37) Dreybrodt, W.; Lauckner, J.; Liu, Z. H.; Svensson, U.; Buhmann, D. *Geochim. Cosmochim. Acta* **1996**, *60*, 3375−3381.

(38) NIST Chemistry Webbook at URL: http://webbook.nist.gov/chemistry/.

(39) Karagulian, F.; Rossi, M. *J. Phys. Chem. Chem. Phys.* **2005**, *7*, 3150−3162.

(40) Moore, M. H.; Khanna, R. K. *Spectrochim. Acta* **1991**, *47A*, 255.

(41) Hage, W.; Hallbrucker, A.; Mayer, E. *J. Am. Chem. Soc.* **1993**, *115*, 8427.

(42) Hage, W.; Hallbrucker, A.; Mayer, E. *J. Chem. Soc., Faraday Trans.* **1996**, *92*, 3197.

(43) Loerting, T.; Tautermann, C.; Kroemer, R. T.; Kohl, I.; Hallbrucker, A.; Mayer, E.; Liedl, K. R. *Angew. Chem., Int. Ed.* **2000**, *39*, 891.

(44) Bonasoni, P.; Cristofanelli, P.; Calzoari, F.; Bonafé, U.; Evangelisti, F.; Stohl, A.; Zauli Sajani, S.; van Dingenen, R.; Colombo, T.; Balkanski, Y. *Atmos. Chem. Phys.* **2004**, *4*, 1201−1215.

(45) Leclaire, A.; Borel, M. M. *Acta Crystallogr. Sect. B−Struct. Sci.* **1977**, *33*, 1608−1610.

(46) King, K. D.; Golden, D. M.; Spokes, G. N.; Benson, S. W. *Int. J. Chem. Kinet.* **1971**, *3*, 411−426.

(47) Koch, T. G.; Rossi, M. *J. Phys. Chem. Chem. Phys.* **1999**, *1*, 2687−2694.

(48) Aguzzi, A.; Rossi, M. J. *Phys. Chem. Chem. Phys.* **2001**, *3*, 3707−3716.